JTTEE5 9:389-393

Base-Metal Saturation of Refractory Carbide Coatings Produced by Enhanced Ceramic Jets in Electrothermally Exploded Powder Spray

Hideki Tamura and Masanobu Itaya

(Submitted 11 May 1999; in revised form 10 December 1999)

Tungsten carbide and tantalum carbide were sprayed onto substrates of mild steel by the electrothermally exploded powder spray (ELTEPS) process. High-speed x-ray radiography revealed that tungsten-carbide jets of molten particles guided inside a nozzle exhibited denser flow than unguided jets at the substrate. The velocity of the jet was approximately 800 m/s at the early stage of jetting. The ceramic coatings obtained from the guided spray consisted of carbides of a few to tens of micrometers in size, which were saturated by the base metal up to the top of the coating. The coatings exhibited diffusion of the sprayed ceramics and base metal at the interface of the deposit and substrate. The enhancement of the jet flow formed a microstructure of the ceramic coating, which was saturated by the base metal even without post heat treatment.

Keywords ceramic jet, diffusion, electrothermal explosion, metallurgical bond, saturation, tantalum carbide, tungsten carbide

1. Introduction

Refractory ceramics and metals have been used as spray materials due to their resistance against abrasive wear and corrosion. The densification and interparticle bond in the coatings are needed to obtain the intrinsic properties of the spray materials. In conventional spray methods, post heat treatment has been employed to decrease cracks and pores by filling nickel alloys and to enhance interparticle bonding by diffusion.[1,2,3] These processes enhanced the coating hardness and wear resistance. Metallurgical bonding at the interface between the coatings and substrates caused by elemental diffusion and mechanical anchoring of the metals increased the adhesion strength of the coatings. The post laser treatment[4] and spray-synchronized laser heating[5,6] controlled the substrate temperature and have also been effective in enhancing the hardness and adhesion of the coatings.

The electrothermally exploded powder spray (ELTEPS) can produce dense deposits of refractory ceramics of electrically conductive carbides and borides without any sintering agents and post heat treatment.[7,8,9] According to the spray condition in the ELTEPS, some of the deposits are characterized with elemental codiffusion at the interfaces or the saturation of base metals up to the coating top surfaces even without any post heat treatment. Based on observation of the structure obtained for titanium boride and nitride coatings, melting, stirring, and capillary movement of substrate metals would be caused by the successive impact of molten ceramic droplets.[10,11]

Hideki Tamura and **Masanobu Itaya,** Department of Materials Science and Engineering, Tokyo Institute of Technology, Yokohama 226-8502, Japan. Contact e-mail: tamura@iron.materia.titech.ac.jp.

The ELTEPS process provides the ceramic feedstock with adequate energy for melting and a jetting velocity of several hundred meters per second.[11] The deposition rate and temperature of the molten ceramics determines the physical processes that occur at the substrate surface and, therefore, the coating structure. In this article, the ceramic jet is guided to substrates to increase the deposition rate. The guidance is characterized by means of a time-resolved observation employing flash x-ray radiography. The coating structure is related to the enhancement of jet flow.

2. Experimental Setup

The ELTEPS process is performed with an electric circuit consisting of a large capacitor and a vacuum chamber in which a powder container is installed between a pair of electrical contacts.[8,10,11] Metal substrates were placed on a holder in the chamber. The powder charged in the container was tungsten carbide, WC (Japan New Metals Co., Ltd., particle size: less than 45 μm, purity: 99.7%, Osaka, Japan), of 2.9×10^{-3} kg, or tantalum carbide, TaC (Japan New Metals Co., Ltd., particle size: less than 45 μm, purity: 99.5%), of 2.4×10^{-3} kg. The powder was packed in the container with a relative density of approximately 50% under an argon atmosphere. The container consisted of an inner polyethylene tube and an outer metal tube with a 16 mm OD. The metal tube had a window of 5×30 mm on its side, which faced the substrate holder.

The Joule heat supplied to the powder was estimated by measuring the voltage and current applied to the powder.[7,8] Figure 1 shows a schematic view of a plane crossing perpendicularly the axis and center of the powder container. A pair of flash x-ray tubes (Scandiflash model 150, Uppsala, Sweden) was placed on a plane facing the container at the standoff distance of 400 mm. The tubes were used in a soft x-ray mode with a pulse width of 35 ns and an x-ray source of 1 mml focal spot size. A substrate holder and a pair of x-ray films (Eastman Kodak Co., model DEF-5, Rochester, NY) were placed perpendicular to the viewing plane at distances of 80 and 400 mm, respectively, from the container axis. Cham-

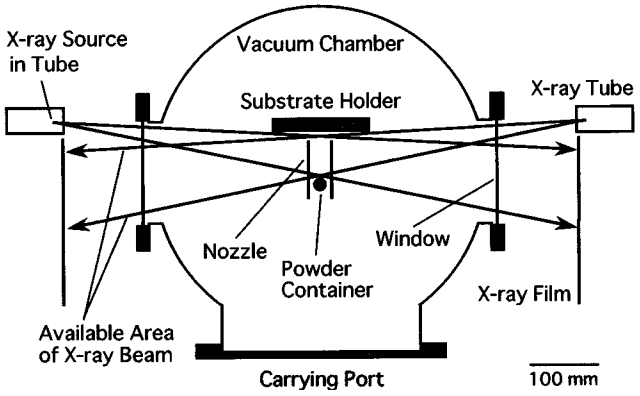

Fig. 1 Schematic of an experimental setup for x-ray radiography. The view is on a plane crossing perpendicularly the axis and center of the po wder container

ber windows and film cases were made of acrylonitrile-butadiene-styrene plates with thicknesses of 6 and 1 mm, respectively. The chamber was filled with nitrogen at 6.7×10^3 Pa.

In order to guide a ceramic jet coming from the container window, a nozzle made of polyethyleneterephthalate thin film was installed in the container. The nozzle was shaped into a tube. The section perpendicular to the tube axis was shaped elliptically. The ellipse had two kinds of radii, *i.e.*, large and small, of 25 and 18 mm. The long radius was placed on the container axis. The nozzle ended 65 mm from the container axis. The nozzle wall thickness was designed to allow the passage of soft x-rays with adequate intensity onto the films and to guide a ceramic jet. Mirror-polished mild-steel substrates were fixed on the holder facing the nozzle. The micromorphology and constituent elements of the coatings obtained were characterized by scanning electron microscopy (SEM, JEOL Co. model JSM-5310, Tokyo) and an electron probe microanalyzer (EPMA, Shimazu Co. model: EPMA-1400, Tokyo, Japan). The crystal phases were investigated using an x-ray diffractometer (XRD, Mac Science model M18XHF, Japan).

3. Experimental Results and Discussion

3.1 Behavior of Ceramic Jets

When the capacitor of the ELTEPS circuit charged at 8.3 kV started to discharge, the powder was immediately Joule-heated by electric current. Figure 2(a) shows typical waveforms of the voltage applied to the electric contacts of the chamber and of the current flowing in the WC powder. The time-varying apparent resistance of the powder was estimated from the voltage and current[7] and is shown in Fig. 2(b). The Joule heat supplied was evaluated from the time integration of the power, which was calculated from the resistance and current and is shown in Fig. 2(c). According to prior work,[11] the rapid decrease of resistance occurred at 69 μs and, marked by β, corresponds to the beginning of a large ejection, *i.e.*, jetting of the ceramic powder heated with high resistivity. The Joule heat supplied until that time is 11.8 kJ, which corresponds to 2.9 times the theoretical energy of 4.1 kJ necessary to melt the powder. The total energy given

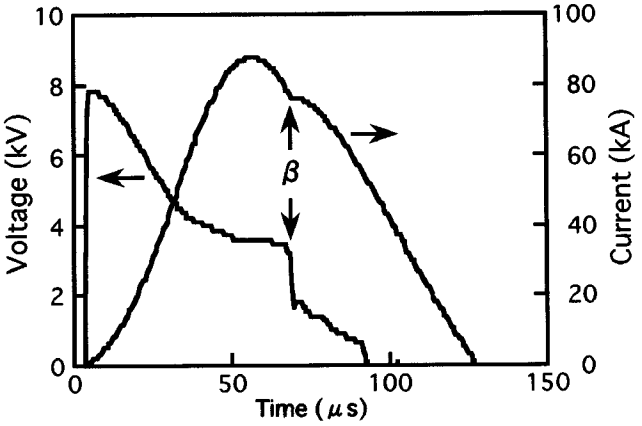

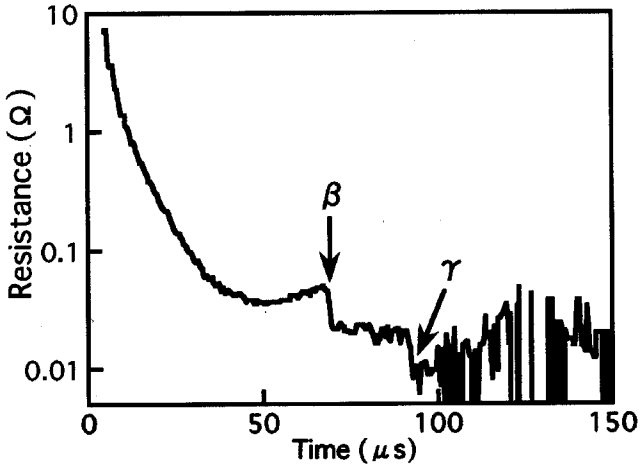

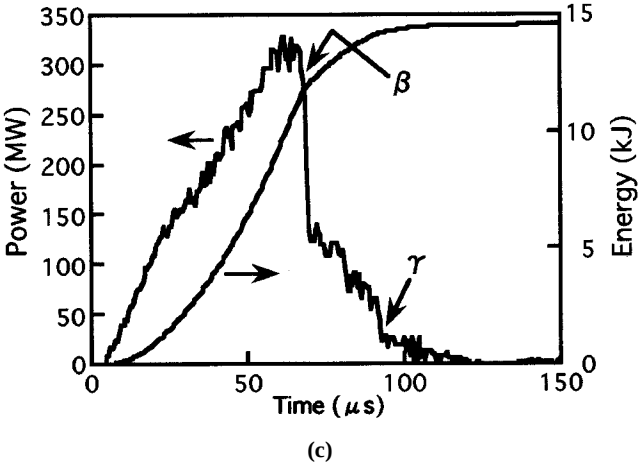

Fig. 2 Electrical characteristics of the ELTEPS of tungsten carbide. (**a**) The applied voltage and current as a function of time. (**b**) The apparent resistance of the powder. (**c**) The electric power and Joule heat supplied

to the powder is calculated to be 14.2 kJ at 93 μs, indicated by the γ symbol.

The guidance of jetting is characterized in comparison with the behavior of unguided systems, *i.e.*, free jetting. Figure 3

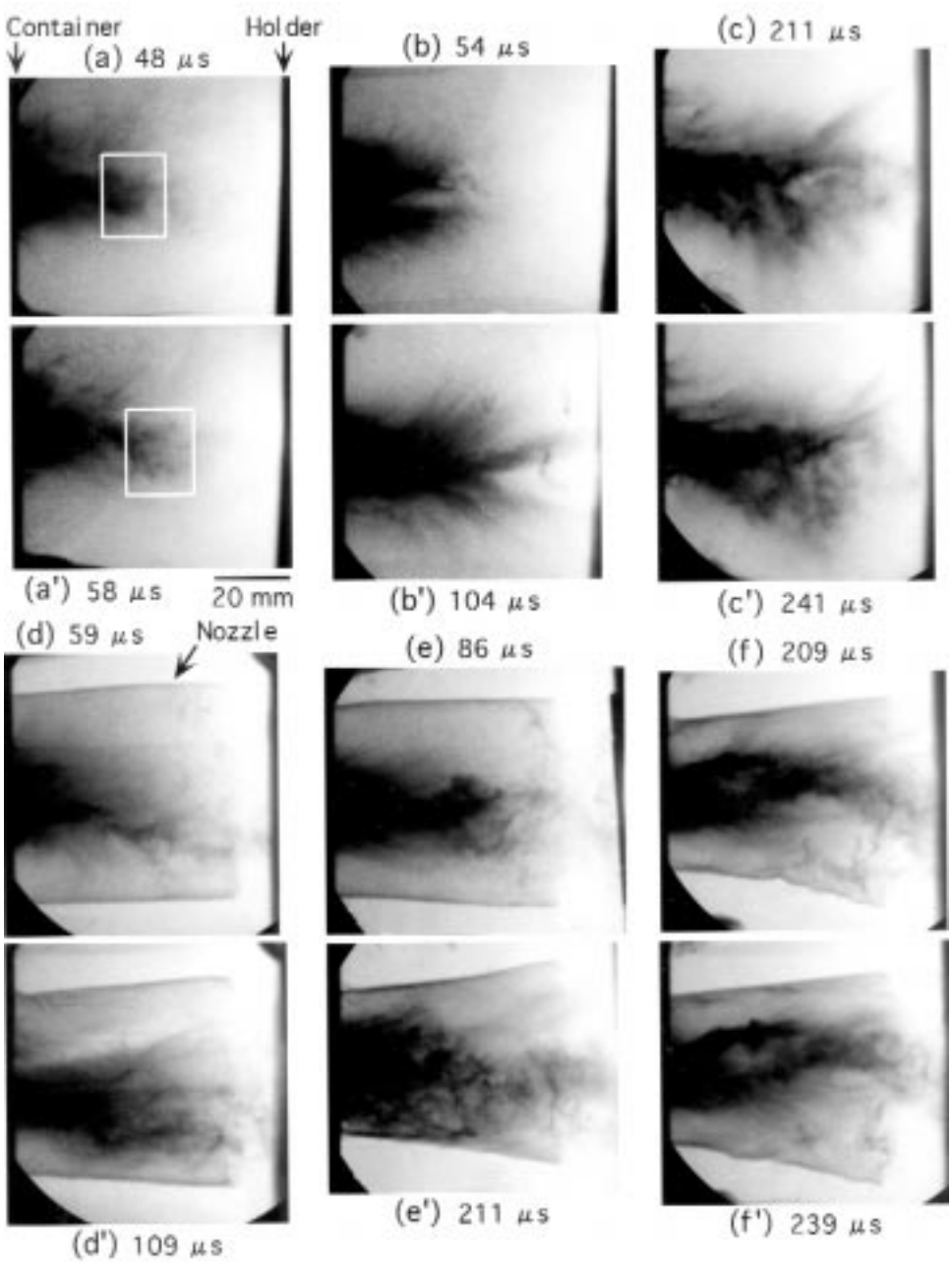

Fig. 3 Soft x-ray shadowgraphs of tungsten carbide jets. Three different sprays conducted by free jetting are shown in three image pairs of (**a**) and (**a′**), (**b**) and (**b′**), and (**c**) and (**c′**). Part of the shadow, which is surrounded by a white square in (**a**), moved to another location indicated in (**a′**). Another three different jets, which were nozzle-guided, are shown in image pairs of (**d**) and (**d′**), (**e**) and (**e′**), and (**f**) and (**f′**). The times indicated originated from each onset of the jetting. The scale corresponds to the unit in length on a plane, which was perpendicular to the substrate holder and included the powder-container axis

shows six pairs of radiographs, *i.e.*, shadowgraphs of the free and guided spray jets. Figure 3(a) and (a′) were taken at different times of 48 and 58 μs respectively, originating from the onset of free jetting. The jet is distinguished by a faint shadow extending from the powder container standing at the left-hand side to the substrate holder at the right-hand side. It is seen that part of the shadow surrounded by a white square in Fig. 3(a) moved to another location indicated in (a′) after 10 μs. The jetting velocity of that part is approximately 800 m/s. Figure 3(b) and (b′) show the change of another jet over a 50 μs interval. The latter shows the narrow condensation of the jet close to the substrate holder and other faint groups extending upward or downward. Another jet captured after 200 μs from its onset also exhibited a faint condensation diverging outward, as shown in Fig. 3(c) and (c′). The electrical characteristics regarding energy supply in these sprays are summarized in Table 1. According to these data, the energy given to the powder until the onset of jetting and the total energy supplied average 11.3 and 13.3 kJ, re-

spectively, with a divergence of 10% for both the free and guided jets shown in Fig. 3.

The early stage of a guided jet is shown in Fig. 3(d) and (d′), which correspond approximately to Fig. 3(b) and (b′), respectively, for the free jet with respect to the time after onset. A faint shadow is seen in front of the holder even at 59 μs. During the latter 50 μs, that shadow enlarged more than 40 mm along the holder surface. However, there is no shadow coming through the nozzle wall. Thus, the jet was guided inside the nozzle and sprayed toward the substrate, while the free jet diverged outward, as seen in Fig. 3(b′). The velocity of the condensed part of a guided jet had been observed to be approximately 800 m/s, based on another pair of radiographs taken at the early stage, not shown here. The faint jet of condensed matter had already filled the space in front of the substrate at the time of 86 μs, as seen in Fig. 3(e). A dense part of the jet had been formed in that space during another 125 μs, as shown in Fig. 3(e′). The electrical characteristics followed by this jetting have been shown in Fig. 2. Another set of radiographs shown in Fig. 3(f) and (f′) also exhibits a dense jet facing the substrate. The jet was still guided inside the nozzle, while the free jets shown in Fig. 3(c) and (c′) diverged faintly. Although there is no leakage of the jet out of the nozzle wall, the deformation of the nozzle base is seen and was caused due to the jet extending perpendicularly to the plane of the photograph. Hence, the nozzle is effective in enhancing the amount of jet flow onto the substrate.

Table 1 Electrical characteristics regarding energy supply in the tungsten-carbide sprays shown in Fig. 3

Spray	Duration of heating before jetting, μs	Energy supplied before jetting, kJ	Duration of energy supply, μs	Total energy supplied, kJ
(a)	65	10.1	96	14.1
(b)	72	12.4	83	13.8
(c)	70	10.7	89	12.2
(d)	68	11.5	92	13.6
(e)	69	11.8	93	14.2
(f)	72	11.5	76	12.0

Note: Spray is identified by the figure number in Fig. 3

3.2 Microstructures of Enhanced Spray Coatings

Figure 4(a) shows the SEM image of the cross section of a tungsten-carbide coating, which was obtained on a mild-steel substrate by the enhanced spray with total Joule heat of 13.5 kJ. The XRD analysis conducted on a coating top surface had already revealed the diffraction peaks corresponding only to the crystal phases of WC, WC_{1-X}, W_2C, and iron, while the diffraction of the cubic WC_{1-X} was much stronger than the others. Thus, decarburization was observed. The elemental analysis of tungsten on the cross section indicates that these carbides exist inside the coating, and it is shown in Fig. 4(b). The bright areas are rich in tungsten. The iron of the substrate was also analyzed, and it is mapped in Fig. 4(c). According to the comparison of the SEM image with the element distributions, it is found that the carbide particles of a few to tens of micrometers in size were saturated by iron, *i.e.*, the base metal. Although the deposit ranged 90 μm in thickness, such saturation of the substrate material reached the top surface of the coating, which is identified on the depth profile of iron in Fig. 4(d). The profile was based on the accumulation of the specific x-ray detection over the area of Fig. 4(c). At the interface of the coating and substrate, the mutual element diffusion of tungsten and iron ranges from several to 20 μm. This saturated microstructure had not been found in any coatings obtained by free, unguided spray jets of tungsten carbide. A monolithic coating of tungsten carbide discretely laid on a mild steel by a free jet can be seen in prior work.[9]

This type of composite made of ceramics saturated with base metals has been found in other coatings of tantalum carbide onto aluminum,[8] titanium carbide onto mild steel,[9] titanium boride onto mild steel,[10] and a composite of titanium boride and nitride onto mild steel and aluminum.[11] The process of these phenomena has been proposed as follows:[11] the jet composed of molten ceramic particle deposits due to successive particle impact on the metal substrate. The surface begins to melt by heat conduction and is stirred by successive impact. Thus, mixing of the molten materials occurs. Although the ceramics should solidify and recrystallize faster than the metal during the cooling phase, the metal would still be molten and saturate the interparticle space of the ceramics up to the top surface of the deposit. The saturation range depends on the deposition rate of the ceramic jet, which is determined by the amount of the jet flow coming onto the substrate.

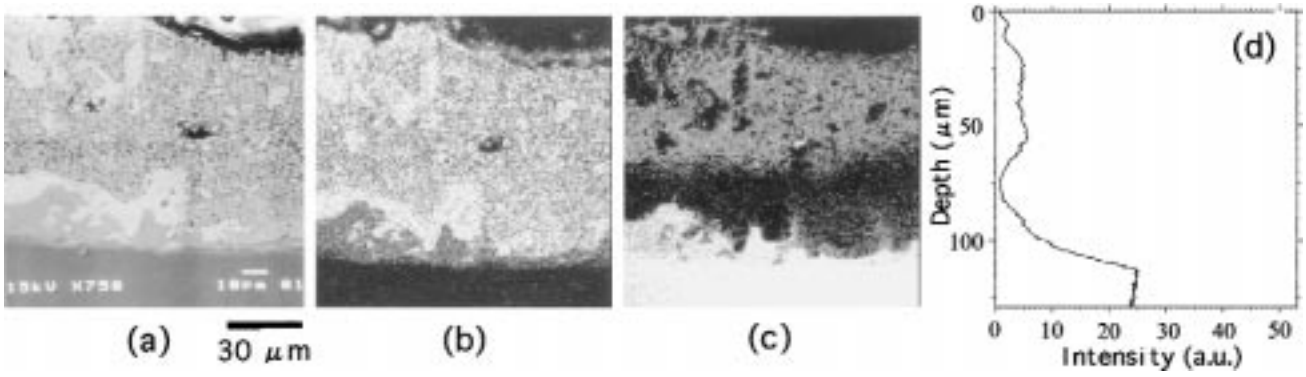

Fig. 4 (**a**) SEM image of a cross section of tungsten-carbide coating obtained on a mild-steel substrate. (**b**) Tungsten element map on the view of (**a**). The bright area is rich in the analyzed element. (**c**) Iron element map. (**d**) Depth profile of iron accumulated over the map of (**c**)

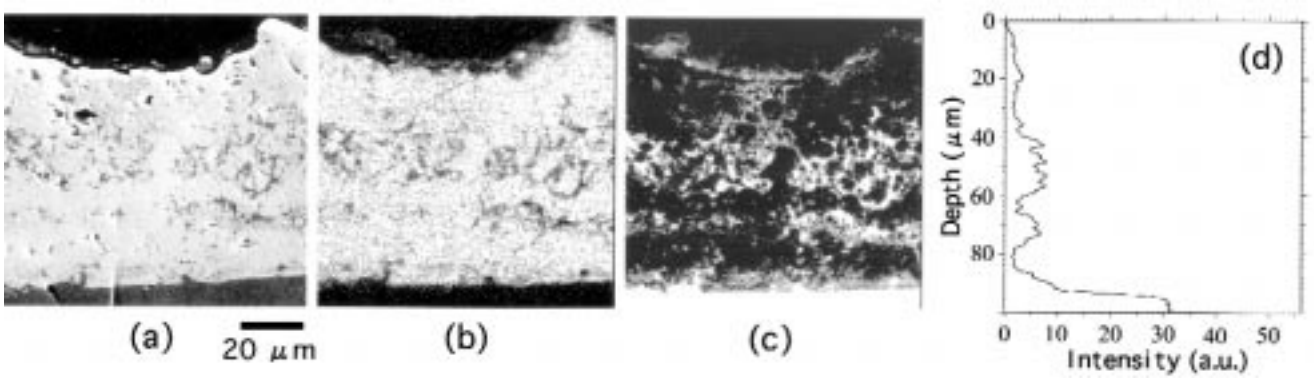

Fig. 5 (**a**) SEM image of a cross section of tantalum-carbide coating obtained on a mild-steel substrate. (**b**) Tantalum element map on the view of (**a**). The bright area is rich in the analyzed element. (**c**) Iron element map. (*d*) Depth profile of iron accumulated over the map of (**c**)

A nozzle-enhanced tantalum carbide jet was used to form another composite of sprayed ceramic and a mild-steel substrate. The total energy of 13.3 kJ was supplied to the TaC jet, which is 2.7 times the theoretical energy to melt the powder.[8] Figure 5 shows the SEM image and element distributions on a coating cross section. The XRD analysis exhibited only the two phases of cubic TaC_x and iron. The decarburization for the carbon content of 0.87 was estimated from the analysis considering the relationship between the carbon content and lattice constant.[12] The coating has a thickness of 70 μm and a base-metal saturation up to 40 μm according to the depth profile of iron. At the interface of the coating and substrate, the mutual diffusion of tantalum and iron ranges 10 μm. A free-jet coating of TaC,[9] however, had not included as much saturation as this enhanced-jet coating. The jet enhancement influenced the spray and increased the deposit yield up to 40 wt.% of the starting material.

4. Conclusions

The spray was guided by a nozzle to the substrate to increase the deposition rate of sprayed ceramics onto metal substrates. A nozzle made of thin plastic film could control the jetting direction of molten tungsten carbide, which was generated under electrothermal explosion of the ceramic powder. Such nozzle guidance was effective in enhancing the amount of the jet flow reaching the substrate. The jetting velocity of the carbide reached 800 m/s at the early stage of the spray process, at which time the ceramic feedstock was Joule-heated up to about three times the theoretical energy to melt the ceramics.

Such enhancement of the flow resulted in microstructures of the tungsten-carbide deposit saturated by a base metal of mild steel without any post treatment. The deposit was 90 μm in thickness and the base metal was observed at the top surface of the deposit. Nozzle-sprayed tantalum carbide was also saturated with the base metal. These coatings, in addition, revealed element diffusion at the interface of the deposit and substrate with no pores or cracks. Another effect of the jet guidance was to increase the deposition efficiency. Decarburization was also observed in both carbides.

Acknowledgments

This work was supported by a Grant-in-Aid for Exploratory Research No. 09875175 of the Ministry of Education, Science, Sports and Culture in Japan, and the authors thank Japan New Metals Co., Ltd. for supplying the powders of tungsten carbide and tantalum carbide.

References

1. H. Hayashi, H. Haraguchi, H. Ito, and O. Nakano: in *Spray: Meeting the Challenges of the 21st Century*, C. Coddet, ed., ASM International, Materials Park, OH, 1998, vol. 1, p 181-85.
2. H. Era, F. Otsubo, and K. Kishitake: in *Spray: Meeting the Challenges of the 21st Century*, C. Coddet, ed., ASM International, Materials Park, OH, 1998, vol. 1, p 711-16.
3. C. Gaudin, P. Prince, P. Jacquot, D. Rivolet, and J.P. Duhamel: in *Spray: Meeting the Challenges of the 21st Century*, C. Coddet, ed., ASM International, Materials Park, OH, 1998, vol. 2, p 1387-92.
4. T. Otmianowski, B. Antoszewski, and W. Zorawski: in *Spray: Meeting the Challenges of the 21st Century*, C. Coddet, ed., ASM International, Materials Park, OH, 1998, vol. 2, p 1333-36.
5. C. Coddet, G. Montavon, T. Marchionet, and O. Freneaux: in *Spray: Meeting the Challenges of the 21st Century*, C. Coddet, ed., ASM International, Materials Park, OH, 1998, vol. 2, p 1321-25.
6. N. Eguchi, Z. Zhou, H. Shirasawa, and A. Ohmori: : in *Spray: Meeting the Challenges of the 21st Century*, C. Coddet, ed., ASM International, Materials Park, OH, 1998, vol. 2, p 1517-22.
7. H. Tamura, M. Nagahama, Y. Tanabe, and A.B. Sawaoka: *J. Appl. Phys.*, 1994, vol. 75, p 4695-4703.
8. H. Tamura, M. Konoue, and A.B. Sawaoka: *J. Thermal Spray Technol.*, 1997, vol. 6, p 463-68.
9. T. Soda, H. Tamura, and A.B. Sawaoka: in *Thermal Spray: Meeting the Challenges of the 21st Century*, C. Coddet, ed., ASM International, Materials Park, OH, 1998, vol. 2, p 1351-56.
10. Y. Ikeda, H. Tamura, and A.B. Sawaoka: *Rev. High Pressure Sci. Technol.*, 1998, vol. 7, p 1472-74.
11. T. Kodama, Y. Ikeda, and H. Tamura: *J. Thermal Spray Technol.*, 1999, vol. 8, p 537-44.
12. E.K. Storms: in *The Refractory Carbides*, J.L. Margrave, ed., Academic Press, New York, NY, 1967, p 84 and 93.